Article

SPR-Enhanced Au@Fe$_3$O$_4$ Nanozyme for the Detection of Hydroquinone

Bin Zhang, Xiaoming Wang, Wei Hu, Yiquan Liao, Yichang He, Bohua Dong, Minggang Zhao * and Ye Ma *

Department of Materials Science and Engineering, Ocean University of China, Qingdao 266100, China
* Correspondence: zhaomg@ouc.edu.cn (M.Z.); maye@ouc.edu.cn (Y.M.)

Abstract: Artificial nanozymes that are based on ferric oxides have drawn enormous attention due to their high stability, high efficiency, and low cost as compared with natural enzymes. Due to the unique optical plasmonic properties, gold nanoparticles (Au NPs) have been widely utilized in the fields of colorimetric, Raman, and fluorescence sensing. In this work, a photo-responsive Au@Fe$_3$O$_4$ nanozyme is prepared with outstanding peroxidase-like activity. The hot electrons of Au NPs that are excited by a surface plasmon resonance (SPR) effect of NPs improve the catalytic activity of Au@Fe$_3$O$_4$ in oxidizing 3,3′,5,5′-tetramethylbenzidine (TMB) and the detection of hydroquinone (HQ). The magnetic separation and reusability of the nanozyme further lower its costs. The detection linear range of the sensor is 0–30 μM and the lowest detection limit is 0.29 μM. Especially in the detection of real water samples, a good recovery rate is obtained, which provides promising references for the development of the HQ detection technology in seawater.

Keywords: gold nanoparticle; surface plasmon resonance; nanozyme; colorimetric

1. Introduction

The survival of living organisms is highly dependent on water resources. However, economic development has led to serious water pollution. Hydroquinone (HQ), as an important chemical raw material, has been widely used in various industrial sectors. According to the regulations of the US Environmental Protection Agency, HQ can cause irreversible damage to the human body even at a trace level of 3.5 mg/L, and it is difficult to degrade in the aquatic ecological environment [1]. Therefore, the accurate detection of HQ in water environments is urgent. At present, a variety of methods for HQ detection have been developed, including the electrochemical method, spectrophotometry, and the fluorescence method, but most of these methods have complicated instruments and operation and take a long time [2]. Therefore, alternative methods that are more intuitive, rapid, and sensitive need to be developed. Colorimetric sensing is a good candidate with the advantages of the visualization of experimental results, simple operation, and low cost [3]. As colorimetric sensing is a technology based on the measurement of colored compounds under visible light, the development of specific and efficient catalysts for colored substances is a very critical step [4].

Artificial nanozymes based on nanomaterials have been developed to catalyze various chromogenic substrates and construct corresponding colorimetric sensors, which have received great attention due to their high stability, high efficiency, low cost, and easy modification [5]. Researchers have developed a variety of oxidase-like or nanozymes based on noble metal-based nanomaterials, metal oxides, and carbon materials. Although the catalytic efficiency of many nanozymes has exceeded that of native enzymes, there is still a need for new nanozymes with a higher catalytic activity in the trace analytical detection at nM level. When using various nanozymes for sensing analysis, researchers found that the performance of light-responsive nanozymes was generally better than that of light-inert nanozymes, such as carbon nitride, PSMOF and CeO$_2$/CoO [6]. However,

in the absence of light, most light-triggered nanozymes will lose their catalytic ability, thus limiting their application in the dark. Therefore, improving catalytic efficiency by light while maintaining catalytic capacity in the dark is a key direction for the future development of multifunctional nanozymes.

Due to their photo-responsiveness, good electrical conductivity, high specific surface area, and excellent catalytic performance, Au NPs have good prospects in the development of high-sensitivity colorimetric sensors. Researchers confirmed that under acidic conditions, Au nanozymes exhibit peroxidase-like activity that catalyzes the conversion of H_2O_2 to hydroxyl radicals ($\bullet OH$) [7]. Moreover, under the incident light irradiation, the internal electrons of Au NPs gain energy to escape from the surface and produce SPR. As an excitation hot electron, it can stay on the surface of the NPs for a long time. It can provide a large number of electrons in the catalytic reaction and act as a fast electron transfer channel, which greatly improves the catalytic performance of nanozymes [8].

At present, researchers have utilized various nanozymes for biosensing applications, such as graphene [9], $NiCo_2O_4@MnO_2$ [1], Fe_3O_4 [10,11], etc. Fe_3O_4 has been widely used in photocatalysis, biosensing, and drug delivery due to its strong magnetic effect and easy recycling [12,13]. Fe_3O_4 contains Fe^{2+}/Fe^{3+} active ion pairs, which exhibit peroxidase-like activity and have significant advantages in promoting REDOX reactions [14]. Most importantly, optimal $Au@Fe_3O_4$ can generate hot electrons under the action of photocatalysis, and the photogenerated electrons actively participate in the generation of $O_2\bullet-$ and $\bullet OH$ and the oxidation of TMB, which can significantly improve its efficiency.

In this work, we synthesized an $Au@Fe_3O_4$ nanocomposite that exhibits peroxidase-like activity. Under light irradiation, the catalytic performance of $Au@Fe_3O_4$ peroxidase-like nanozyme can be further improved. In addition, unlike most photo-catalysts, the peroxidase-like activity can also be maintained in dark conditions. In the proof-of-concept colorimetric detection of HQ, the minimum detection limit could reach 0.29 μM, and it was successfully applied to tap water and seawater. Moreover, the $Au@Fe_3O_4$ peroxidases can also be recovered by magnetic separation, and the economic cost of practical applications can be further reduced.

2. Materials and Methods

2.1. Chemicals and Characterizations

Sodium citrate, gold chloride trihydrate ($HAuCl_4\cdot 3H_2O$), hydroxylamine (NH_2OH), ferrosoferric oxide (Fe_3O_4), 3-aminopropyl triethoxysilane (APTES), 3,3′,5,5′-tetramethylbenzidine (TMB), lithium chloride (LiCl), hydrochloric acid (HCl), sodium hydroxide (NaOH), disodium hydrogen phosphate (Na_2HPO_4), mercuric nitrate ($Hg(NO_3)_2$), cadmium nitrate ($Cd(NO_3)_2$), nickel nitrate ($Ni(NO_3)_2$), copper sulfate ($CuSO_4$), and lead nitrate ($Pb(NO_3)_2$) were all purchased from Shanghai China Aladdin Chemical Co., LTD. Sodium chloride (NaCl) and potassium chloride (KCl), ferrous chloride ($FeCl_2$), phenol, resorcinol (RC), o-nitro resorcinol (ONP), and hydroquinone (HQ) were purchased from China Shanghai MacLean Biochemical Co., LTD. The ultraviolet spectrophotometer used was from China Shanghai Yuan Analysis Instrument Co., LTD. Ultra-pure (UP) water with a resistivity of 18.25 MΩ·cm was used for the experiment.

The morphology and particle size of the samples were characterized by scanning electron microscopy (SEM, SU8010). The magnetic properties of the samples were determined by electron paramagnetic resonance spectroscopy (EPR, Brooker A300) and vibrating sample magnetometry (VSM, LakeShore7404), and the pH value of the solution was measured by a PH-3D pH meter from China Shanghai Precision Scientific Instrument Co., LTD. The UV–visible absorption spectra were recorded by a UV–visible spectrophotometer (UV-8000).

2.2. Preparation of Gold NPs

The classical method to synthesize gold nanomaterials was the seed growth method, whereby spherical 16 nm gold NPs were prepared by a reduction method. Firstly, 0.8 mL 5%wt aqueous solution of $HAuCl_4 \cdot 3H_2O$ and 400 mL ultra-pure water were mixed in a three-way flask, heated, and stirred to boil under magnetic stirrers, and kept boiling for 30 min. Then, 8 mL 1%wt sodium citrate solution was added and reacted for 30 min to completely reduce it. After cooling for 4–5 h, 16 nm gold NPs can be obtained, and their characteristic absorption peak was about 520 nm. A volume of 30 mL of 16 nm Au NPs was titrated to 300 mL with ultrapure water. NH_2OH solution was added. After strong stirring for a period of time, 520μL 5%wt aqueous solution of $HAuCl_4 \cdot 3H_2O$ was added into the mixed solution, and the reaction lasted for 15 min. Finally, gold NPs at 40 nm, with characteristic absorption peaks of around 525 nm, were obtained.

2.3. Preparation of Au@Fe$_3$O$_4$ Nanozymes

An amount of 45 mg of Fe_3O_4 was mixed with 3 mL 3-aminopropyltriethoxysilane reagent (APTES) in 30 mL absolute ethanol. After sonication for 5 min, the cells were subjected to mechanical stirring for 6 h at room temperature. Sialylation modification of Fe_3O_4 solution was obtained by redispersing the product in 30 mL of water by magnetic separation.

30 mL of aminated Fe_3O_4 was mixed with 30 mL of prepared Au NPs and mechanically stirred at room temperature for 3 h. The product was re-dispersed in 15 mL of water by magnetic separation to obtain Au@Fe_3O_4 solution.

2.4. Materials Characterization

The samples were characterized by SEM, UV–Vis absorption spectroscopy, X-ray diffractometer, energy dispersive spectrometer (EDS), electron paramagnetic resonance spectroscopy (EPR), hysteresis loop measurement (VSM), and X-ray photoelectron spectroscopy (XPS). SEM was used to characterize the morphology and size of Au@Fe_3O_4 nanocomposites. The composition of the composite was analyzed using an X-ray diffractometer with analysis conditions set at $2\theta = 20–80°$, scanning speed of $10°$/min, and Cu Kα radiation. XPS was used to further characterize the chemical composition of the composite, and a C1s line with a binding energy of 284.8 eV was used for calibration. EDS was used to analyze the elemental information of Au@Fe_3O_4 nanocomposites. ●OH production was verified using EPR. The optical properties of Au@Fe_3O_4 nanocomposites were tested using VSM. The properties of the materials were tested using UV–Vis absorption spectroscopy.

3. Results

3.1. Material Characterization and Analysis

The Au@Fe_3O_4 nanocomposite synthesis process is shown in Figure 1. First, APTES was modified on the Fe_3O_4 surface to make it positively charged, while the -COOH of the citrate on the NPs can be dissociated into -COO$^-$, which renders the NPs negatively charged. Subsequently, the negatively charged Au NPs are assembled in situ on amino-functionalized Fe_3O_4 via electrostatic interactions to form Au@Fe_3O_4 nanozymes. As shown in Figure 2a, the prepared Au NPs have a diameter of about 16 nm, with good homogeneity [15]. Figure 2b shows that Au NPs are uniformly distributed on the Fe_3O_4 surface. Moreover, no obvious large-scale agglomeration of Au NPs was observed. As shown in Figure 2c–e, the results of EDS elemental mapping analysis showed that Au, Fe, and O elements were uniformly distributed, further proving the successful synthesis of Au@Fe_3O_4 nanozymes.
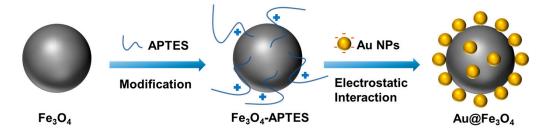
Figure 1. Schematic diagram of the synthesis of Au@Fe$_3$O$_4$ nanocomposites.

Figure 2. (**a**) SEM image of 16 nm Au NPs. (**b**) SEM image of Au@Fe$_3$O$_4$ nanozymes and EDS element mapping image of Fe (**c**), O (**d**), and Au (**e**) of Au@Fe$_3$O$_4$ nanozymes. Scale bar, 100 nm.

XPS was used to characterize the chemical states of Au, Fe, and O in Au@Fe$_3$O$_4$. The broad spectrum in Figure S1a shows binding energy peaks for Au4f, C1s, O1s, and Fe 2p, respectively. As shown in Figure S1b, the binding energies corresponding to the characteristic peaks of Au $4f_{5/2}$ and Au $4f_{7/2}$ are 86.4 eV and 82.7 eV, respectively, and the appearance of Au 4f indicates that Au is a zero-valent state [16]. As shown in Figure S1c, the binding energies corresponding to the characteristic peaks of Fe $2p_{1/2}$ and Fe $2p_{3/2}$ are 725.3 eV and 709.7 eV, respectively, in line with the standard data of Fe$_3$O$_4$ [17]. As shown in Figure S1d, the binding energy corresponding to the characteristic peak of O1s is 528.9 eV, which is a typical metal–oxygen bond [18]. The XRD patterns are shown in Figure S2. The diffraction peaks at 38.1° and 45.1° correspond to the (111) and (200) crystal planes of Au [19], respectively. The diffraction peaks at 30.2°, 35.5°, 43.3°, 53.6°, 57.1°, and 62.8° correspond to (220), (311), (400), (422), (511), and (440) crystal planes of Fe$_3$O$_4$, respectively [20]. The results show that Au@Fe$_3$O$_4$ nanozymes have been successfully prepared.

As shown in Figure S3a, neither Fe$_3$O$_4$ nor Au@Fe$_3$O$_4$ nanocomposites have remanence or coercivity at 300 K, which indicates that both samples are paramagnetic at room temperature. The saturation magnetization of Fe$_3$O$_4$ and Au@Fe$_3$O$_4$ is 81.3 emu/g and 78.9 emu/g, respectively. Figure S3b demonstrates the enrichment and redispersion process of Au@Fe$_3$O$_4$ nanocomposites. After magnet placement, Au@Fe$_3$O$_4$ nanocomposites were rapidly enriched on the side of the glass bottle within 30 s. After the removal of the magnet,

the Au@Fe$_3$O$_4$ nanocomposite can be redispersed by shaking or ultrasonic vibration. The test results show that the Au@Fe$_3$O$_4$ nanocomposite still retains good magnetic properties and can be recycled by magnetic separation.

3.2. Au@Fe$_3$O$_4$ Enzyme Mimetic Activity of Nanozymes

Researchers have found that Au nanozymes and Fe$_3$O$_4$ nanozymes can catalyze the decomposition of H$_2$O$_2$ to produce •OH under acidic conditions, showing peroxidase-like activity [7]. Au NPs can catalyze the O–O bond cleavage of H$_2$O$_2$ to form two •OH [21]. Fe$_3$O$_4$ nanozymes contain Fe^{2+}/Fe^{3+} active ion pairs that decompose H$_2$O$_2$ into •OH by Fenton mechanism [22]. In colorimetric detection, •OH can catalyze the conversion of the oxidase substrate TMB to the blue charge–transfer complex oxTMB. Importantly, the transfer of electrons from the nanozyme to the reaction medium is able to promote the generation of •OH [23,24]. For example, Abir Swaidan et al. [25]. found that a large amount of electron transfer between Cr^{3+} and Cr^{6+} could accelerate the decomposition of H$_2$O$_2$ to •OH, thereby enhancing the ability to oxidize TMB. Therefore, we use the SPR effect of Au NPs to stimulate a large number of high-energy electrons. At the same time, Au NPs can also act as a fast electron transfer channel [8], Fe^{2+}/Fe^{3+} active ion pairs participate in REDOX reactions, and multi-factor cooperation promotes the decomposition of H$_2$O$_2$ to •OH. After that, TMB was catalyzed to oxTMB by one-electron transfer, and the color of the solution changed from colorless to blue. The catalytic reaction process is shown in Equations (1)–(3) [1,14,26] and Figure 3. HQ is strongly reducing, which can reduce blue oxTMB to colorless TMB, so as to construct a colorimetric sensing platform for detecting HQ. The whole catalytic process is an electron transfer process from MB to H$_2$O$_2$ with the assistance of Au and Fe^{2+}/Fe^{3+} as a medium.

$$H_2O_2 \xrightarrow{Au/e^-} \bullet OH \tag{1}$$

$$Fe^{2+} + H_2O_2 + H^+ \rightarrow Fe^{3+} + \bullet OH + H_2O \tag{2}$$

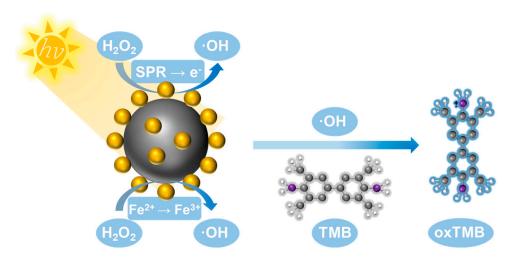$$\bullet OH + TMB \rightarrow oxTMB + H_2O \tag{3}$$

Figure 3. Schematic diagram of catalytic reaction process.

The Au@Fe$_3$O$_4$ peroxidase-like enzyme mimetic activity was assessed by catalyzing the oxidation of TMB, which has a characteristic absorption peak at 652 nm. The prepared samples were subjected to the catalytic oxidation of TMB in 0.2 M Na$_2$HPO$_4$-CA buffer at pH = 4.0. To demonstrate the peroxidase-like activity of Au@Fe$_3$O$_4$ nanozymes, we tested the oxidation of TMB in the presence and absence of H$_2$O$_2$. As shown in Figure 4a, the

absorbance is almost a horizontal line in the absence of H_2O_2, indicating that Au@Fe$_3$O$_4$ nanozymes, Au NPs, and Fe$_3$O$_4$ NPs cannot directly oxidize TMB. However, in the presence of H_2O_2, Au@Fe$_3$O$_4$ showed a higher peroxidase activity compared to the addition of Au NPs and Fe$_3$O$_4$ NPs only. This is because the Au@Fe$_3$O$_4$ peroxidase-like enzyme couples the catalytic ability of both Au and Fe^{2+}/Fe^{3+} ion pairs, thus achieving high catalytic efficiency for TMB. More importantly, the catalytic performance of Au@Fe$_3$O$_4$ nanozymes will be further improved under the simulated illumination condition of a xenon lamp, which is closely related to the SPR effect of Au NPs. The internal electrons of Au NPs escape from the surface with photon energy, which is manifested as the excited hot electrons residing on the surface of the NPs, and can provide a large number of electrons in the catalytic reaction. At the same time, Au NP can provide a fast electron transfer channel for the catalytic reaction [8], and both can cooperate to improve the catalytic performance of nanozymes. It is now generally accepted that peroxidase mimics can catalyze the decomposition of H_2O_2 to produce •OH. To further investigate the mechanism of action of the photo-enhanced peroxidase, •OH was characterized by electron paramagnetic resonance. As shown in Figure 4b, •OH could not be produced in solution in the absence of Au@Fe$_3$O$_4$ nanozymes. Under dark conditions, the characteristic 5, 5-dimethyl-1-pyrroline N-oxide (DMPO)-•OH peak appeared after the addition of Au@Fe$_3$O$_4$, confirming the production of •OH and the peroxidase-like activity of Au@Fe$_3$O$_4$. Under the simulated illumination condition of the xenon lamp, the signal intensity of •OH was significantly enhanced, indicating that the large number of hot electrons excited by the SPR effect promoted the conversion of H_2O_2 to •OH. These results indicate that the light-induced SPR effect can significantly enhance the catalytic oxidation ability of Au@Fe$_3$O$_4$ nanozymes.
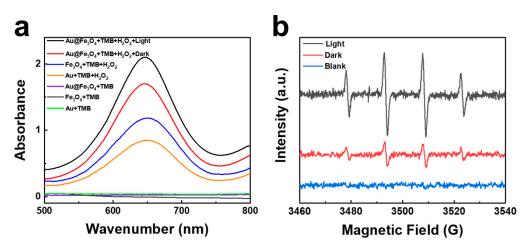

Figure 4. (**a**) UV–Vis absorption spectra in different reaction systems: Au@Fe$_3$O$_4$ nanozymes+ TMB+H_2O_2+light (black), Au@Fe$_3$O$_4$ nanozymes+TMB+H_2O_2 (red), Fe$_3$O$_4$+TMB+H_2O_2 (blue), Au+TMB+H_2O_2 (orange), Au@Fe$_3$O$_4$ nanozymes+TMB (purple), Fe$_3$O$_4$+TMB (gray), Au@+TMB (green). (**b**) DMPO-EPR spin-trapping spectra of Au@Fe$_3$O$_4$ nanozymes for detection of •OH. Reaction conditions: 100 µg/mL nanozymes (either Au@Fe$_3$O$_4$, Au NPs, or Fe$_3$O$_4$), 0.5 mM TMB, 70 mM H_2O_2, 0.2 M Na$_2$HPO$_4$-CA buffer (pH = 4.0), 12 min reaction time, pH = 4, 25 °C, 300 W xenon lamp for light conditions.

The experimental conditions for the catalytic oxidation of TMB by Au@Fe$_3$O$_4$ nanozymes were next optimized. First, the effect of buffer solution pH on the catalytic activity of Au@Fe$_3$O$_4$ nanozymes was investigated. Figure 5a shows that Au@Fe$_3$O$_4$ exhibits the best relative catalytic activity at pH = 4.0. Therefore, the effect of temperature on Au@Fe$_3$O$_4$ catalytic activity was further tested at pH = 4.0 maintenance. As shown in Figure 5b, the material exhibited the best relative activity when the temperature was around 25 °C. Then, the effect of Au@Fe$_3$O$_4$ concentration on the catalytic performance was tested at pH 4.0 and a temperature of 25 °C. As shown in Figure 5c, the relative activity

of Au@Fe$_3$O$_4$ increased steadily from 0 µg/mL to 100 µg/mL. In the range of 100 µg/mL to 140 µg/mL, Au@Fe$_3$O$_4$ showed the best relative activity. As shown in Figure 5d, the relative activity gradually increased with the extension of reaction time from 1 to 12 min, and essentially remained stable after 12 min. Based on the above discussion, the optimal reaction pH of Au@Fe$_3$O$_4$ peroxidases was determined to be 4.0, the optimal experimental temperature was 25 °C, the optimal addition concentration was 100 µg/mL, and the optimal reaction time was 12 min.
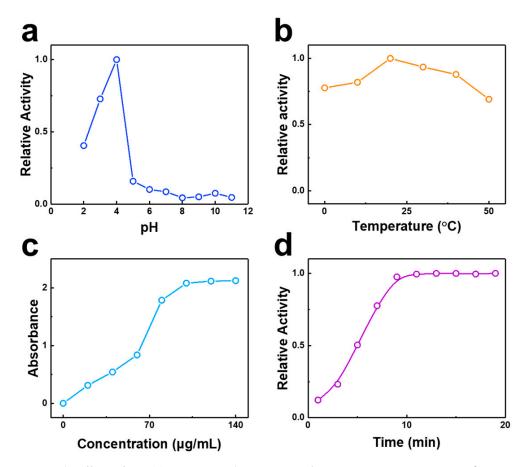

Figure 5. The effects of: pH (**a**) reaction conditions: 100 µg/mL Au@Fe$_3$O$_4$ nanozymes, 25 °C, 12 min; temperature (**b**) 100 µg/mL Au@Fe$_3$O$_4$ nanozymes, 12 min pH = 4; concentration (**c**) 25 °C, 12 min, pH = 4; and reaction time (**d**) 100 µg/mL Au@Fe$_3$O$_4$ nanozymes, 25 °C, pH = 4, on the activity of Au@Fe$_3$O$_4$ nanozymes.

3.3. Colorimetric Detection

First, we detected HQ under dark conditions using the Au@Fe$_3$O$_4$ peroxidase-like enzyme. HQ, which is strongly reducing, can reduce the blue oxTMB solution to a colorless TMB solution. This macroscopic blue bleaching reaction is due to the two-electron reduction in oxTMB by •OH induced by hydroquinone. The physical diagram of the catalytic process and the reaction formula are shown in Figure S4. As shown in Figure 6a, it can be concluded that the peak absorbance at 652 nm decreased with increasing HQ concentration. Figure 6b shows that there is a linear relationship between the peak absorbance and HQ concentration, and the corresponding linear fitting equation is y = −0.0204x + 1.6918 (R^2 = 0.991), and the lowest detection line is 1.24 µM. The above experimental results indicate that the Au@Fe$_3$O$_4$ peroxidase-like enzyme can also be applied to the fading colorimetric detection of HQ under dark conditions.

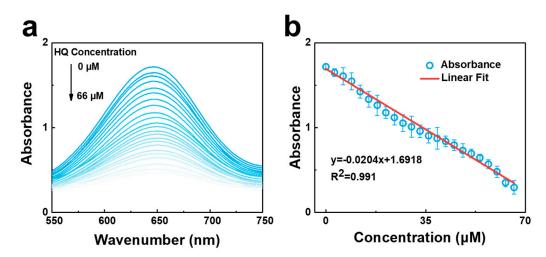**Figure 6.** (**a**) UV–Vis absorption spectra of Au@Fe$_3$O$_4$ nanozymes–TMB colorimetric platform with the presence of 0–45 μM HQ. (**b**) Linear fitting of peak absorbance vs. HQ concentration. Reaction conditions: 100 μg/mL Au@Fe$_3$O$_4$ nanozymes, 0.5 mM TMB, 0.2 M Na$_2$HPO$_4$–CA buffer (pH = 4.0), 12 min, 25 °C, and dark conditions.

Next, HQ was again detected using the Au@Fe$_3$O$_4$ peroxidase under simulated illumination with a 300 W xenon lamp. As shown in Figure 7a, the peak absorbance at 652 nm decreased with increasing HQ concentration, and the initial absorbance and the amount of absorbance change were significantly larger than those under dark conditions. This is because under the light conditions, the photoexcitation SPR effect produces a large number of hot electrons, which makes the content of •OH in the solution higher, and the ability to oxidize TMB is subsequently strengthened, leading to a deeper initial color, that is, a higher absorbance. This was also confirmed by UV–Vis and EPR experiments that simulated the active part of the enzyme. When HQ is added to react with oxTMB, the fading change will be more obvious, that is, it will show a larger amount of absorbance change on the spectrum. Figure 7b shows that there is a linear relationship between the peak absorbance and HQ concentration, and the corresponding linear fitting equation is y = −0.0588x + 2.0249 (R^2 = 0.999), and the lowest detection line is 0.29 μM. Compared with dark detection, the Au@Fe$_3$O$_4$ peroxidase-TMB colorimetric detection platform under light has a higher sensitivity. The above experimental results show that the photoexcitation SPR effect can effectively enhance the colorimetric detection performance of Au@Fe$_3$O$_4$ peroxidases for HQ. The detection range of this experiment is 0–30 μM, and the lowest detection limit is 0.29 μM, which has certain advantages compared with other methods reported in the literature, as shown in Table 1.

The selectivity, repeatability, and stability of the sensor are crucial for practical applications. The selectivity of HQ was determined by the addition of possible interfering substances. As shown in Figure 8a, equal concentrations of phenol, resorcinol (RC), o-nitro resorcinol (ONP), Cl$^-$, NO^{3-}, SO$_4^{2-}$, Cd^{2+}, Ca^{2+}, Cu^{2+}, Fe^{3+}, Hg^{2+}, K$^+$, Na$^+$, Ni^{2+}, and Pb^{2+} were added. It does not substantially interfere with HQ detection, indicating that the Au@Fe$_3$O$_4$ peroxidase-like enzyme has good selectivity. After that, the Au@Fe$_3$O$_4$ peroxidase-like enzyme was added to the TMB solution and its stability was verified using UV–Vis absorption spectroscopy. As shown in Figure S5, its relative activity remained largely unchanged after 12 cycles, indicating a good short-term stability. Similarly, the relative activity of the samples was also largely unchanged over 15 days, indicating a good long-term stability of the material, as shown in Figure 8b. Five batches of Au@Fe$_3$O$_4$ peroxidases were prepared under the same experimental conditions to test their absorbance after catalytic oxidation of TMB. As shown in Figure 8c, the relative activity of the five batches of samples remained essentially unchanged. After that, the reproducibility of the same Au@Fe$_3$O$_4$ class of peroxidase samples was tested. As shown in Figure 8d, the same

Au@Fe$_3$O$_4$ class of peroxidases still maintained a high relative activity after four magnetic separation recoveries, indicating good reproducibility.
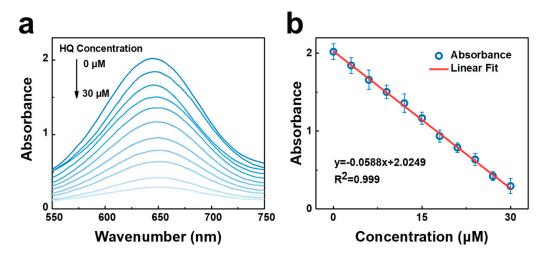

Figure 7. (**a**) UV–Vis absorption spectra of Au@Fe$_3$O$_4$ nanozymes–TMB colorimetric platform with the presence of 0–30 μM HQ. (**b**) Linear fitting of peak absorbance vs. HQ concentration. Reaction conditions: 100 μg/mL Au@Fe$_3$O$_4$ nanozymes, 0.5 mM TMB, 0.2 M Na$_2$HPO$_4$–CA buffer (pH = 4.0), 12 min, 25 °C, and 300 W xenon lamp simulates light conditions.

Table 1. Comparison of the sensing performance of other methods in the detection of HQ.

Methods	Linear Ranges (μM)	LOD (μM)	Reference
colorimetry	1–30	0.8	[27]
colorimetry	2.7–19	1.6	[28]
colorimetry	1–85	0.68	[29]
colorimetry	5–200	3	[30]
electrochemistry	1–10	0.8	[31]
electrochemistry	25–2500	0.61	[32]
electrochemistry	4.6–35.2	1.4	[33]
fluorescence	1–200	0.5	[34]
fluorescence	2.5–27	0.68	[35]
fluorescence	6–100	2.63	[36]
colorimetry	0–66	1.24	this work (dark)
	0–30	0.29	this work (light)

To verify the utility of the Au@Fe$_3$O$_4$ peroxidase, HQ was measured in tap water and seawater, and the recovery was calculated in real water samples. All samples were collected from Qingdao, China. Tap water and seawater samples were filtered using a nylon filter membrane with a pore size of 0.22 μM to remove solid impurities. Amounts of 8 μM, 18 μM, and 29 μM HQ were added to tap water and seawater samples, respectively, and their absorbance was tested using a UV–Vis spectrophotometer, and the measured values were calculated by linear fitting equations. As shown in Table 2, better recoveries were obtained in both tap water and seawater. These results indicate that the Au@Fe$_3$O$_4$ peroxidase-like enzyme has a potential application in the detection of HQ for seawater anti-interference.
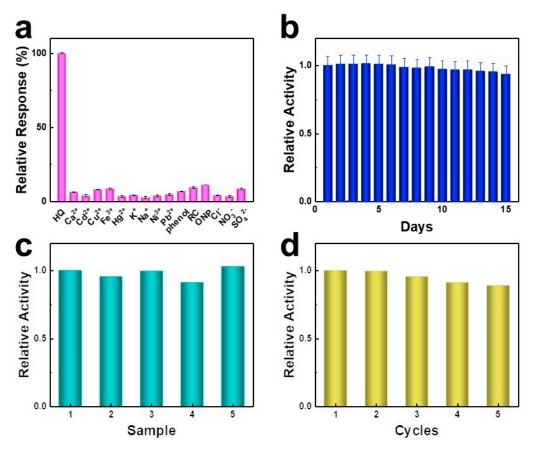
Figure 8. (**a**) The selectivity of Au@Fe$_3$O$_4$ nanozymes-TMB colorimetric platform toward HQ in the presence of other interfering substances (phenol, RC, ONP, Cl$^-$, NO^{3-}, SO$_4{}^{2-}$, Cd^{2+}, Ca^{2+}, Cu^{2+}, Fe^{3+}, Hg^{2+}, K$^+$, Na$^+$, Ni^{2+}, and Pb^{2+}). (**b**) The long-term stability of Au@Fe$_3$O$_4$ nanozymes. (**c**) The reproducibility of Au@Fe$_3$O$_4$ nanozymes prepared in different batches. (**d**) The relative activity of Au@Fe$_3$O$_4$ nanozymes after multiple magnetic separations and recycling.

Table 2. Measuring HQ in tap water and sea water.

Sample	Added (μM)	Detected (μM)	Recovery (%)	RSD (%)
Tap Water	8	7.5 ± 0.13	93.8	1.7
	18	18.3 ± 0.10	101.7	0.6
	29	28.6 ± 0.23	102.1	0.8
Sea Water	8	7.7 ± 0.11	96.3	1.4
	18	17.9 ± 0.19	99.5	1.1
	29	29.9 ± 0.22	103.1	0.8

4. Conclusions

In this study, the enhancement of Au@Fe$_3$O$_4$ peroxidase-like activity by SPR effect was successfully applied to the colorimetric detection of HQ in seawater. The results show that Au NPs excite hot electrons under light irradiation and provide a large number of electrons for the catalytic reaction. At the same time, Au NPs can be used as fast charge transfer channels, while theAu@Fe$_3$O$_4$) with a large specific surface area can provide more active sites. Under the synergistic effect of multiple factors, the ability of Au@Fe$_3$O$_4$ peroxidase to catalyze the oxidation of TMB was significantly enhanced, and the sensitivity of colorimetric detection was improved. Moreover, the Au@Fe$_3$O$_4$ peroxidase-like nanozyme still has a certain colorimetric detection ability under dark conditions. Au@Fe$_3$O$_4$ peroxidases can

also be recovered by magnetic separation, and the economic cost of practical applications can be further reduced. The experimental results show that the minimum detection limit of HQ detection by this method can reach 0.29 μM, which has advantages compared with other methods reported in the literature. In addition, a good recovery rate was obtained in the detection of real water samples, which can provide some reference for the development of HQ detection technology in seawater. In future research, Au NPs can be coupled with other nanomaterials to construct heterostructures or metal organic frameworks (MOFs), which can further improve the performance of plasmonic or SERS-based sensors [37,38].

Supplementary Materials: The following supporting information can be downloaded at: https://www.mdpi.com/article/10.3390/chemosensors11070392/s1, Figure S1: XPS characterization; Figure S2: XRD characterization; Figure S3: Magnetization curves of Fe_3O_4 and $Au@Fe_3O_4$ nanocomposites; Figure S4: Catalytic process; Figure S5: Short-term stability.

Author Contributions: B.Z., Data curation; formal analysis; visualization; writing—original draft; X.W., data curation; formal analysis; W.H., data curation; writing—review and editing; Y.L. and Y.H., formal analysis; B.D., methodology; writing—review and editing; Y.M. and M.Z., funding acquisition; conceptualization; supervision. All authors have read and agreed to the published version of the manuscript.

Institutional Review Board Statement: Not applicable.

Informed Consent Statement: Not applicable.

Data Availability Statement: The data presented in this study are available on request from the corresponding author.

Conflicts of Interest: The authors declare no conflict of interest. The funding sponsors had no role in the design of the study; in the collection, analyses, or interpretation of data; in the writing of the manuscript, and in the decision to publish the results.

References

1. Ma, Y.; Zhu, M.Y.; He, Q.; Zhao, M.G.; Cui, H.Z. Photoenhanced Oxidase-Peroxidase-like $NiCo_2O_4@MnO_2$ Nanozymes for Colorimetric Detection of Hydroquinone. *ACS Sustain. Chem. Eng.* **2022**, *10*, 5651–5658. [CrossRef]
2. Yao, Y.Z.; Liu, Y.C.; Yang, Z.S. A novel electrochemical sensor based on a glassy carbon electrode modified with Cu-MWCNT nanocomposites for determination of hydroquinone. *Anal. Methods UK* **2016**, *8*, 2568–2575. [CrossRef]
3. Zhao, X.; Lyu, H.Y.; Yao, X.X.; Xu, C.; Liu, Q.Y.; Liu, Z.X.; Zhang, X.X.; Zhang, X. Hydroquinone colorimetric sensing based on platinum deposited on CdS nanorods as peroxidase mimics. *Microchim. Acta* **2020**, *187*, 587. [CrossRef] [PubMed]
4. Xi, Z.; Wei, K.C.; Wang, Q.X.; Kim, M.J.; Sun, S.H.; Fung, V.; Xia, X.H. Nickel-Platinum Nanoparticles as Peroxidase Mimics with a Record High Catalytic Efficiency. *J. Am. Chem. Soc.* **2021**, *143*, 2660–2664. [CrossRef]
5. Masud, M.K.; Kim, J.; Billah, M.M.; Wood, K.; Shiddiky, M.J.A.; Nguyen, N.T.; Parsapur, R.K.; Kaneti, Y.V.; Alshehri, A.A.; Alghamidi, Y.G.; et al. Nanoarchitectured peroxidase-mimetic nanozymes: Mesoporous nanocrystalline alpha-or gamma-iron oxide? *J. Mater. Chem. B* **2019**, *7*, 5412–5422. [CrossRef]
6. Zhang, J.Y.; Liu, J.W. Light-activated nanozymes: Catalytic mechanisms and applications. *Nanoscale* **2020**, *12*, 2914–2923. [CrossRef]
7. Wang, Z.R.; Zhang, R.F.; Yan, X.Y.; Fan, K.L. Structure and activity of nanozymes: Inspirations for de novo design of nanozymes. *Mater. Today* **2020**, *41*, 81–119. [CrossRef]
8. Kuo, C.H.; Li, W.K.; Pahalagedara, L.; El-Sawy, A.M.; Kriz, D.; Genz, N.; Guild, C.; Ressler, T.; Suib, S.L.; He, J. Understanding the Role of Gold Nanoparticles in Enhancing the Catalytic Activity of Manganese Oxides in Water Oxidation Reactions. *Angew. Chem. Int. Ed.* **2015**, *54*, 2345–2350. [CrossRef]
9. Chen, Y.; He, Z.L.; Ding, S.Q.; Wang, M.; Liu, H.L.; Hou, M.X.; Chen, X.; Gao, J.; Wang, L.X.; Wong, C.P. Facilely preparing lignin-derived graphene-ferroferric oxide nanocomposites by flash Joule heating method. *Res. Chem. Intermediat.* **2023**, *49*, 589–601. [CrossRef]
10. Sun, H.Y.; Jiao, X.L.; Han, Y.Y.; Jiang, Z.; Chen, D.R. Synthesis of Fe_3O_4-Au Nanocomposites with Enhanced Peroxidase-Like Activity. *Eur. J. Inorg. Chem.* **2013**, *2013*, 109–114. [CrossRef]

11. Yang, D.; Wang, L.X.; Jia, T.T.; Lian, T.; Yang, K.D.; Li, X.H.; Wang, X.; Xue, C.H. Au/Fe₃O₄-based nanozymes with peroxidase-like activity integrated in immunochromatographic strips for highly-sensitive biomarker detection. *Anal. Methods-UK* **2023**, *15*, 663–674. [CrossRef] [PubMed]

12. Ivanchenko, M.; Nooshnab, V.; Myers, A.F.; Large, N.; Evangelista, A.J.; Jing, H. Enhanced dual plasmonic photocatalysis through plasmonic coupling in eccentric noble metal-nonstoichiometric copper chalcogenide hetero-nanostructures. *Nano Res.* **2022**, *15*, 1579–1586. [CrossRef]

13. Ahmadivand, A.; Gerislioglu, B.; Manickam, P.; Kaushik, A.; Bhansali, S.; Nair, M.; Pala, N. Rapid Detection of Infectious Envelope Proteins by Magnetoplasmonic Toroidal Metasensors. *ACS Sens.* **2017**, *2*, 1359–1368. [CrossRef] [PubMed]

14. Jiang, D.W.; Ni, D.L.; Rosenkrans, Z.T.; Huang, P.; Yan, X.Y.; Cai, W.B. Nanozyme: New horizons for responsive biomedical applications. *Chem. Soc. Rev.* **2019**, *48*, 3683–3704. [CrossRef]

15. Hafez, M.E.; Ma, H.; Ma, W.; Long, Y.T. Unveiling the Intrinsic Catalytic Activities of Single-Gold-Nanoparticle-Based Enzyme Mimetics. *Angew. Chem. Int. Ed.* **2019**, *58*, 6327–6332. [CrossRef]

16. Wang, L.; Luo, J.; Fan, Q.; Suzuki, M.; Suzuki, I.S.; Engelhard, M.H.; Lin, Y.; Kim, N.; Wang, J.Q.; Zhong, C.J. Monodispersed core-shell Fe3O4@Au nanoparticles. *J. Phys. Chem. B* **2005**, *109*, 21593–21601. [CrossRef]

17. Xing, Y.; Jin, Y.Y.; Si, J.C.; Peng, M.L.; Wang, X.F.; Chen, C.; Cui, Y.L. Controllable synthesis and characterization of Fe₃O₄/Au composite nanoparticles. *J. Magn. Magn. Mater.* **2015**, *380*, 150–156. [CrossRef]

18. Yang, Y.T.; Jiang, K.D.; Guo, J.; Li, J.; Peng, X.L.; Hong, B.; Wang, X.Q.; Ge, H.L. Facile fabrication of Au/Fe₃O₄ nanocomposites as excellent nanocatalyst for ultrafast recyclable reduction of 4-nitropheol. *Chem. Eng. J.* **2020**, *381*, 122596. [CrossRef]

19. Muzzi, B.; Albino, M.; Gabbani, A.; Omelyanchik, A.; Kozenkova, E.; Petrecca, M.; Innocenti, C.; Balica, E.; Lavacchi, A.; Scavone, F.; et al. Star-Shaped Magnetic-Plasmonic Au@Fe₃O₄ Nano-Heterostructures for Photothermal Therapy. *ACS Appl. Mater. Inter.* **2022**, *14*, 29087–29098. [CrossRef]

20. Lin, F.H.; Peng, H.H.; Yang, Y.H.; Doong, R.A. Size and morphological effect of Au-Fe₃O₄ heterostructures on magnetic resonance imaging. *J. Nanopart. Res.* **2013**, *15*, 2139. [CrossRef]

21. Zhang, Z.Y.; Berg, A.; Levanon, H.; Fessenden, R.W.; Meisel, D. On the interactions of free radicals with gold nanoparticles. *J. Am. Chem. Soc.* **2003**, *125*, 7959–7963. [CrossRef] [PubMed]

22. Chaibakhsh, N.; Moradi-Shoeili, Z. Enzyme mimetic activities of spinel substituted nanoferrites (MFe₂O₄): A review of synthesis, mechanism and potential applications. *Mater. Sci. Eng. C-Mater.* **2019**, *99*, 1424–1447. [CrossRef] [PubMed]

23. Borthakur, P.; Boruah, P.K.; Das, M.R.; Artemkina, S.B.; Poltarak, P.A.; Fedorov, V.E. Metal free MoS₂ 2D sheets as a peroxidase enzyme and visible-light-induced photocatalyst towards detection and reduction of Cr(vi) ions. *New J. Chem.* **2018**, *42*, 16919–16929. [CrossRef]

24. Borthakur, P.; Das, M.R.; Szunerits, S.; Boukherroub, R. CuS Decorated Functionalized Reduced Graphene Oxide: A Dual Responsive Nanozyme for Selective Detection and Photoreduction of Cr(VI) in an Aqueous Medium. *ACS Sustain. Chem. Eng.* **2019**, *7*, 16131–16143. [CrossRef]

25. Swaidan, A.; Borthakur, P.; Boruah, P.K.; Das, M.R.; Barras, A.; Hamieh, S.; Toufaily, J.; Hamieh, T.; Szunerits, S.; Boukherroub, R. A facile preparation of CuS-BSA nanocomposite as enzyme mimics: Application for selective and sensitive sensing of Cr(VI) ions. *Sens. Actuat. B-Chem.* **2019**, *294*, 253–262. [CrossRef]

26. Mu, M.; Wen, S.S.; Hu, S.Z.; Zhao, B.; Song, W. Putting surface-enhanced Raman spectroscopy to work for nanozyme research: Methods, materials and applications. *Trac-Trend Anal. Chem.* **2022**, *152*, 116603. [CrossRef]

27. Zhang, L.P.; Xing, Y.P.; Liu, L.H.; Zhou, X.H.; Shi, H.C. Fenton reaction-triggered colorimetric detection of phenols in water samples using unmodified gold nanoparticles. *Sens. Actuat. B-Chem.* **2016**, *225*, 593–599. [CrossRef]

28. Wu, T.; Ma, Z.; Li, P.; Lu, Q.; Liu, M.; Li, H.; Zhang, Y.; Yao, S. Bifunctional colorimetric biosensors via regulation of the dual nanoenzyme activity of carbonized FeCo-ZIF. *Sens. Actuators B Chem.* **2019**, *290*, 357–363. [CrossRef]

29. Zheng, X.; Liu, Z.; Lian, Q.; Liu, H.; Chen, L.; Zhou, L.; Jiang, Y.; Gao, J. Preparation of Flower-like NiMnO₃ as Oxidase Mimetics for Colorimetric Detection of Hydroquinone. *ACS Sustain. Chem. Eng.* **2021**, *9*, 12766–12778. [CrossRef]

30. Zhuang, Z.; Zhang, C.; Yu, Z.; Liu, W.; Zhong, Y.; Zhang, J.; Xu, Z. Turn-on colorimetric detection of hydroquinone based on Au/CuO nanocomposite nanozyme. *Microchim. Acta* **2022**, *189*, 293. [CrossRef]

31. Li, S.J.; Xing, Y.; Wang, G.F. A graphene-based electrochemical sensor for sensitive and selective determination of hydroquinone. *Microchim. Acta* **2012**, *176*, 163–168. [CrossRef]

32. Ahmad, K.; Kumar, P.; Mobin, S.M. A highly sensitive and selective hydroquinone sensor based on a newly designed N-rGO/SrZrO₃ composite. *Nanoscale Adv.* **2020**, *2*, 502–511. [CrossRef]

33. Pérez-Ràfols, C.; Guo, K.; Alba, M.; Toh, R.J.; Serrano, N.; Voelcker, N.H.; Prieto-Simón, B. Carbon-stabilized porous silicon as novel voltammetric sensor platforms. *Electrochim. Acta* **2021**, *377*, 138077. [CrossRef]

34. Huang, H.; Xu, M.; Gao, Y.; Wang, G.; Su, X. Water-soluble fluorescent conjugated polymer-enzyme hybrid system for the determination of both hydroquinone and hydrogen peroxide. *Talanta* **2011**, *86*, 164–169. [CrossRef] [PubMed]

35. Yuan, X.; Wang, B.; Yan, C.; Lv, W.; Ma, Q.; Zheng, B.; Du, J.; Xiao, D. A rapid and simple strategy for discrimination and detection of catechol and hydroquinone by fluorescent silicon nanoparticles. *Microchem. J.* **2020**, *158*, 105263. [CrossRef]

36. Liu, Y.; Wang, Q.; Guo, S.; Jia, P.; Shui, Y.; Yao, S.; Huang, C.; Zhang, M.; Wang, L. Highly selective and sensitive fluorescence detection of hydroquinone using novel silicon quantum dots. *Sens. Actuators B Chem.* **2018**, *275*, 415–421. [CrossRef]

37. Shumskaya, A.; Korolkov, I.; Rogachev, A.; Ignatovich, Z.; Kozlovskiy, A.; Zdorovets, M.; Anisovich, M.; Bashouti, M.; Shalabny, A.; Busool, R.; et al. Synthesis of Ni@Au core-shell magnetic nanotubes for bioapplication and SERS detection. *Colloid Surf. A* **2021**, *626*, 127077. [CrossRef]

38. Huang, Y.; Gu, Y.Q.; Liu, X.Y.; Deng, T.T.; Dai, S.; Qu, J.F.; Yang, G.H.; Qu, L.L. Reusable ring-like Fe_3O_4/Au nanozymes with enhanced peroxidase-like activities for colorimetric-SERS dual-mode sensing of biomolecules in human blood. *Biosens Bioelectron* **2022**, *209*, 114253. [CrossRef]